EAI Endorsed Transactions
on AI and Robotics

Research Article EAI.EU

LQG, PID controller, ANN for single axis gimbal actuator

Nguyen Cong Danh[1,*]

[1] The single author, District 2, HCMC, Vietnam

Abstract

Gimbal or other stable platforms have structures that move according to its functions. This is for the purpose of keeping track of the goals to the fullest. Tracking targets can become difficult as the subject moves further and further away and they are out of the gimbal's allowable viewing range. Besides, under the influence of noise signals form outside space, it becomes even more difficult to observe the gimbal's targets. To overcome above disadvantages, this paper is presented an adjustment method to limit above risks. Adjusting Linear Quadratic Gaussian (LQG) for expensive gimbal systems, noise signals are processed purely by Kalman filters to improve the function of observing targets. In addition, proportional-integral-derivative (PID) controller, artificial neural network in this case is also considered to verify the effectiveness of control methods listed below. In particular, ANN is the most effective control method today to deal with unwanted signals. These unwanted signals can cause worsening conditions during the operation of systems.Therefore, artificial network (ANN) is a solution to information and communication security problems. Simulation is done by Matlab. Novelty of the work: no previous research has been published for this genre. The study of this genre with the use of artificial intelligence is suggestive of the study of artificial intellligence technologies at a higher level. This category is also a suggestion for studying a smoother control method based on existing data.

Keywords: adjusting LQG, single axis gimbal, Kalman filters, PID controller, ANN.

Received on 21 April 2022, accepted on 18 August 2022, published on 02 September 2022

doi: 10.4108/airo.v1i1.551

1. Introduction

The gimbal is a device that serves many sciences. The target of the objects in sight is the gimbal's operational criteria. The gimbal's payload is usually the equipment that carries a great deal of influence and they are capable of observing the target from a great distance like a radar system, a system of observatories. A gimbal can be installed for all devices in the same system to have a comprehensive view of the objects. A gimbal consists of rings pivoted at right angles to each other. They form a chain of loops connected to each other. This gives flexibility in adjusting a gimbal. A gimbal can stabilize multiple subjects with a single axis of rotation or multiple axes of rotation. In this case, setting up gimbals at each station is not possible in an environment with limited contact area. The uniqueness of this device: it is widely used in scientific fields such as astrology, space science, national defense, security, etc.These fields all need a modern tool so that humans or sensors can observe objects from a distance. Because of the importance of this device in the above areas, research into this category is necessary to have a more in-depth look at this system. In addition, the study of this genre is a suggestion for further research in the future with the great support of increasingly modern automated systems. Modeling control and simulation of two axes gimbal seeker [1] using state-of-the-art controllers is a great idea for the security sector. Modeling control and simulation of two axes gimbal seeker [2] using LQG regulator as presented in this paper is a new research work. Using cascade control

[*] Corresponding author. Email: congdanh.ptithcm@gmail.com

approach [3] for improving three axes gimbal seeker performance is an innovation. Hardware implementation of an ADRC controller [4] on multi-axis gimbal mechanism is promising work.Fractional order [5] of a gimbal platform that PID controller can be applied. Spacecraft angular rates and angular acceleration estimation [6] using a 2 axis gimbal is a pleasant experience. The techniques [7] can be applied to planetary gimbals. Adjusting LQG for internally stabilized platform with actuator saturation [8] is a possible topic in the future. High-precision control [9] for ac-robots is a great research idea. Robust control of magnetically suspended [10] ac-robots is worthy of the author's attention. High-precision anti-disturbance gimbal servo control [11] for ac-robots help readers better understand the functions of the robotic arms. System performance of an internally stabilized [12] ac-robots are a refreshing idea. A two-axis gimbaled sensor system [13] with adjusting LQG is very powerful. Using loop shaping design procedure [14] for a two-axis gimbaled sensor system can be executed. Adjusting the LQG for the gimbal servo system [15] is a fascinating work for the author. Precise control [16] for a two-axis gimbaled sensor system is a new research work that the author looks forward to doing it in the future. Speed tracking control [17] for ac-robots with harmonic drive is an endless source of inspiration. The techniques in [18, 19, 20, 21] can be applied for ac-robots. There are many models applied by modern control algorithms [22, 23, 24]. However, they have not been used artificial intelligence algorithms and the comparison of the superiority of algorithms has not been implemented on previous publications. Generalizing the problems of modern control programs [25] is necessary so that the author can derive the most effective solutions for each specific case. A program that has masterfully guided the operations [26] of a particular object is very interesting and practical. The main contributions of this paper: (i) the author updated the latest controller (PID controller, ANN) at the present time to evaluate the quality of the system under current conditions. (ii) the author used LQG regulator with Kalman filter to handle unwanted noise signals to ensure that the system's orthodox signals have better quality. ANN in this case can replace functions of any part or transfer function in a system if it has been trained before. This is useful in solving security incidents, redundancy works. Core methods are clear in sections 3-5. There are 3 control methods simulated in this paper: LQG, PID controller, ANN. The simulation part is described in detail in Section 6. The theoretical part of LQG regulator is described in detail in Section 4. The theoretical part of ANN is described in detail in Section 5.

2. Modelling of gimbal actuator

The gimbal actuation is generally achieved by using a direct current (DC) motor or brush-less direct current (BLDC) motor of the system. The output angular velocity is measured by using a gyroscope sensor. The stabilization loop of a single axis gimbal actuation system is shown in Fig. 1.

2.1. DC motor model

The DC motor transfer function of the system is given by:

$$\frac{T_m(s)}{U_a(s)} = \frac{K_t}{Ls + R} \tag{1}$$

where $T_m(s)$ and $U_a(s)$ are the torque produced by the DC motor and actuation input respectively of the system. L, R, K_t are defined as inductance, resistance, DC motor torque constant of armature winding of DC motor of the system respectively. The load and motor inertia transfer function is represented by

$$\frac{\omega(s)}{T(s)} = \frac{1}{Js} \tag{2}$$

where, $\omega(s)$ and $T(s) = T_m(s)+T_d(s)$ are the output angular velocity or output angular rate and total torque of load and motor respectively. Td (s) is defined as the load torque disturbance of the system. J is the total inertia of the gimbal of the system. The DC motor transfer function with back electromotive force (EMF) effect of the motor is given by

$$G_m(s) = \frac{\omega(s)}{U(s)} = \frac{K_t}{JLs^2 + JRs + K_t K_e} \tag{3}$$

where, K_e and $U(s)=U_a(s)+ K_e\omega(s)$ are the back EMF constant of DC motor and control input provided by the controller respectively.

2.2. Gryscope model

The gyroscope sensor is used to measure the output angular rate of the gimbal. Typically, a gyroscope model is represented as a second order transfer function given as

$$G_g(s) = \frac{\omega_m(s)}{\omega(s)} = \frac{\omega_n^2}{s^2 + 2\xi\omega_n s + \omega_n^2} \tag{4}$$

where, $\omega_m(s)$, ω_n, and ξ are the measured angular rate, natural frequency, and damping ratio of the gyroscope respectively.

3. Model design

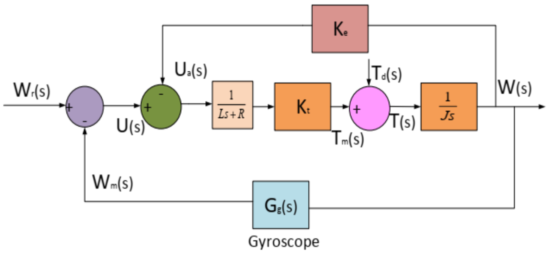

Figure 1. Stabilization loop of a single axis gimbal system.

This system includes the core savings within it:

Box A: 1/ L*s+R
Box B: K_t
Box C: 1/ J*s
Box D: K_e
Box F: $G_g(s)$

Box A is connected in series with Box B. They form Box J. Box J is also connected in series with Box C. They also form Box K. Box K is connected in parallel with Box D so that they form a first sub-closed loop. This sub-closed loop is named $G_m(s)$. $G_m(s)$ is paralleled with $G_g(s)$ and they form a large closed loop. This is the model of the system. The closed loop characteristic equation of gimbal system is writen as: $1+ G_m(s)*G_g(s)=0$

The DC motor transfer function $G_m(s)$ and gyroscope transfer function $G_g(s)$ can again be written as

$$G_m(s) = \frac{0.85}{0.000000345s^2 + 0.05175s + 0.7225} \tag{5}$$

$$G_g(s) = \frac{K_1}{s^2 + b_1 s + b_2} ; G_g(s) = \frac{2500}{s^2 + 70s + 2500} \tag{6}$$

where, by comparing (5) and (6) with (3) and (4) $K_1 = \omega_n^2$, $b_1 = 2\omega_n\xi$, and b_2 = ω_n^2 are obtained. G(s) is the transfer function of the system. G(s) is given

$$G(s) = \frac{G_m(s)}{1 + G_m(s) \times G_g(s)} \tag{7}$$

Table 1. DC motor and Gyroscope specifications

Parameter	Value
Armature resistance (R)	4.5 Ω
Armature inductance (L)	0.003H
Torque constant (K_t)	0.85Nm/A
Back EMF constant(K_e)	0.85V/rad/s
Total inertia (J)	0.0115 kg. m^2
Natural frequency (ω_n)	50 Hz
Damping ratio (ξ)	0.7

4. LQG regulator

LQG is used as one of methods to deal with noise signals. The system must be linear in this case. If the system is not linear, it is necessary to convert the problem to linear form before LQG can be used. Because the result is not as expected when the model is not linear. Therefore, in recent surveys, the author always oriented them to linear to achieve the expected steady state. The author has conducted a review of models with using LQG (Fig 2):

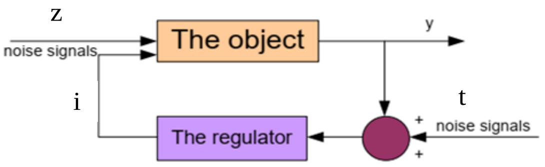

Figure 2. The regulator for the object with noise signals

In figure 2, the subject has noise signals that have affected the input (z) of the object and noise signals (t) have appeared while the author is measuring to collect the data of the system. The goal of this control work is also applied based on the model of Figure 2. The setting of LQG regulator is similar to that of other controllers, that is, it is formed from the construction of control algorithms. The objective of this method is to stabilize the output signals so that they reach a threshold of zero or close to zero. In this model, the input signals are composed of white noise signals (z) and other noise signals (t), the control signal is 'i'. A system of state equations is represented as:

$$\begin{cases} \dot{x} = Lx + Mi + Nz \\ \bar{y} = Fx + Oi + Rz + t \end{cases} \tag{8}$$

LQG contains of a state feedback unit (it's colored in pink) and a Kalman filter (it is colored in green) (Fig. 3).

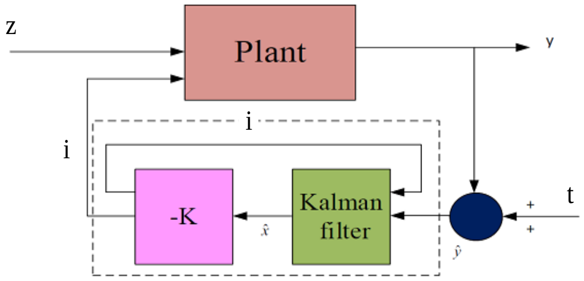

Figure 3. LQG regulator with noise signals (‘z’: the white noise and ‘t’: the color noise signal)

The quality indicator, symbol is (J), (J) is used to find the state feedback matrix $K = lqr(S, H, G, X, F)$

$$J(i) = \int_0^{\infty} \{x^T Gx + 2x^T Fi + i^T Xi\} dt \tag{9}$$

This quality criterion is also used to evaluate under optimal assumptions in a few other cases. It is also used in other controllers subject to accompanying conditions. The composition of these criteria can also be predefined according to the requirements. K is also widely used in optimization controllers. K is commonly known as an integral value in modern controllers and it is often installed at the output of a main controller in models.

The control signal is $i = -K \times \hat{x}$, $\hat{x}$ is inferred for Kalman filter, $\hat{x}$ is output signal of Kalman filter:

$$\dot{\hat{x}} = S\hat{x} + Hu + V(\bar{y} - F\hat{x} - Ou) \tag{10}$$

The value of ‘V’ is the Kalman gain and the value of ‘V ’ is calculated by commands:

[k$_{est}$, V, P]=kalman (sys, G$_n$, X$_n$, F$_n$) (11)

[k$_{est}$, V, P, M, Z]=kalmd (sys, G$_n$, X$_n$, T$_s$) (12)

[k$_{est}$, V, P]=kalman (sys, G$_n$, X$_n$, F$_{n,}$ sensors, known) (13)

[k$_{est}$, V, P, M, Z]=kalman (sys, G$_n$, X$_n$, F$_n$) (14)

where G$_n$, X$_n$, T$_s$ is the variance of the noise signal. $A(zt^T) = G_n$, $A(tt^T) = X_n$, $A(zt^T) = F_n$

k$_{est}$ is the model of Kalman filter.

These commands depend on previously provided data so that the author can execute one of them. Simulation results are the component values of LQG regulator after it has ‘processed’ the model.

Kalman filter calculates $\hat{x}$ to minimize the variance

$$P = \lim_{t\to\infty} A(\{x - \hat{x}\}\{x - \hat{x}\}^T) \tag{15}$$

The equation of state for a regulator (LQG)

$$\frac{d}{dt}\hat{x} = [S - VF - (H - VO)]\hat{x} + V\bar{y} \tag{16}$$

$i = -K\hat{x}$ is established by commands

A=lqgreg (k$_{est}$, k) (17)

A=lqgreg (k$_{est}$, k, ‘current’) (18)

A=lqgreg (k$_{est}$, k, controls) (19)

To find the value of control signal 'i', the author can execute one of the above commands according to the given data. Simulation results are component values of LQG regulator, specifically here a value of a control signal 'i'.
A is the state-space model of a set of LQG, the value of the ouput is ‘i’, the value of the input is $\bar{y}$, the value of the state is $\hat{x}$

A=lqgreg (kest, k, controls) is used for the following model (Fig 4):

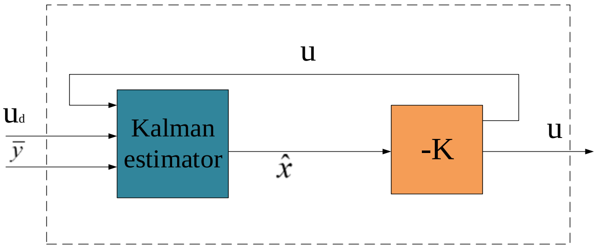

LQG regulator

Figure 4. LQG regulator

Finally, the command is requested:

B= reg (sys, T, U) (20)

B= reg (sys, T, U, sensors, known, controls) (21)

The author established a closed loop with the value of ‘sys’ as the object, the value of ‘T’ is the state feedback matrix, ‘U’ is the state estimation matrix, ‘sensors’ is a subset of outputs, the value of ‘y’ returns to the estimator, ‘known’ are the inputs, ‘i$_d$’ affects the estimator, ‘controls’ are inputs of ‘sys’ that is used for control. To design LQG regulator in this case, the author can execute one of above commands according to the given data. Simulation results are values of LQG regulator.

5. Model with using artificial neural network (ANN)

5.1. An artificial neural network

An artificial neural network (or neural network for short) can be seen as a simple mathematical model of the human brain. Neural networks consist of neurons (processing units) connected to each other by links. Each link is associated with a weight, which characterizes the excitatory or inhibitory properties between neurons.

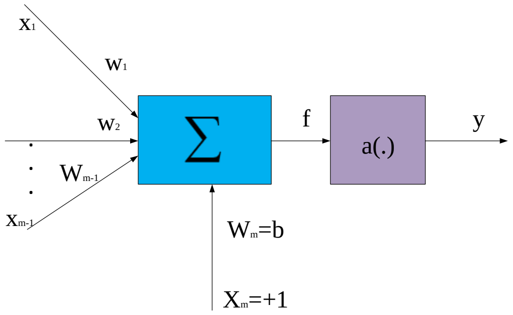

Figure 5. Artificial neurons

Figure 5 has been depicted with a block diagram: there are m-1 inputs, b is the bias level, a(.) is the transfer function from input (f) to output (y).

5.1.1. Input signal

There are (m) input signals, where (m-1) the excitation signal at the input is (x_1, x_2, …, x_{m-1}), they are taken from the output of neurons placed before this neuron or they are taken from other input signal sources. These input excitation signals is passed through a set of weights (w) that characterizes the degree of association between the front neuron is associated with it. A positive association weight corresponds to a restrained synapse. Particularly, the (mth) input signal component (x_m) is called threshold with the value: x_m = +1. The (x_m) signal is passed through the displacement component (bias) b_i : w_m = b. The input processing function is a sum function of the following form:

5.1.1.1. Linear function:

$$f = net = \left(\sum_{j=1}^{m} w_j x_j \right) + w_m b = \left(\sum_{j=1}^{m} w_j x_j \right) + b \qquad (22)$$

5.1.1. 2. Quadratic function:

$$f = net = \left(\sum_{j=1}^{m} w_j x_j^2 \right) + b \qquad (23)$$

5.1.1.3. Spherical function

$$f = net = \left(\rho^{-2} \sum_{j=1}^{m} \left(x_j - w_j \right)^2 \right) + b \qquad (24)$$

The most commonly used input sum function is the linear function

5.1.2. Output of neuron

The output of the neuron is given by the expression: y=a (net)= a (f), where a (.) is the symbol of the conversion function. The conversion function, there is a document also called an activation function or a transfer function, which is responsible for converting the total weight (f) (or net) into an output signal (y). The most commonly used types of conversion functions:

5.1.2.1. Hard limit transfer function:

$$a(f) = step(f) = \begin{cases} 1 & if \quad f \geq 0 \\ 0 & if \quad f < 0 \end{cases} \qquad (25)$$

5.1.2.2. Symmetric hard limit transfer function:

$$a(f) = \mathrm{sgn}(f) = \begin{cases} 1 & if \quad f \geq 0 \\ -1 & if \quad f < 0 \end{cases} \qquad (26)$$

5.1.2.3. Linear transfer function

$$a(f) = (f) \qquad (27)$$

5.1.2.4. Saturation slope function

$$a(f) = \begin{cases} 1 & if \quad f > 1 \\ f & if \quad 0 \leq f \leq 1 \\ 0 & if \quad f < 0 \end{cases} \qquad (28)$$

5.1.2.5. Saturation linear function

$$a(f) = \begin{cases} 1 & if \quad f > 1 \\ f & if \quad 0 \leq |f| \leq 1 \\ -1 & if \quad f < -1 \end{cases} \qquad (29)$$

5.1.2.6. Unipolar sigmoid function

$$a\left(f\right)=\frac{1}{1+e^{-\lambda f}}\quad\left(\lambda>0\right)\tag{30}$$

5.1.2.7. Dipole sigmoid function

$$a\left(f\right)=\frac{2}{1+e^{-\lambda f}}-1\quad\left(\lambda>0\right)\tag{31}$$

Neurons with a transformation function a(.) in the form of unipolar sigmoid or bipolar sigmoid are called Linear Graded Unit (LGU).

5.2. Multilayer feedforward neural network

5.2.1. Multilayer feedforward neural network architecture

Multilayer feedforward network is a feedforward network with two or more layers of processing of neurons. The layer of neurons connected to the input is called the input layer (usually the input layer does not perform processing operations), the layer of neurons connected to the output is called the output layer, the layer of neurons that is not directly connected to the input and the output is called the hidden layer. Connections between of neurons in layers can be complete or incomplete. The algorithm for training the multilayer feedforward network is a backpropagation algorithm. The back-propagation algorithm is implemented in two steps of information transmission. First, the input sample (x(k)) is transmitted from input to output, the result of forward data transmission is to produce the signal (y(k)) at the output of the network. Then, the error as the difference between d(k) and y(k) is propagated back from the output layer back to the previous layer to update the weights of the network. Since the algorithm for training the forward-propagation network is a back-propagation algorithm, this network is also called a back-propagation network.

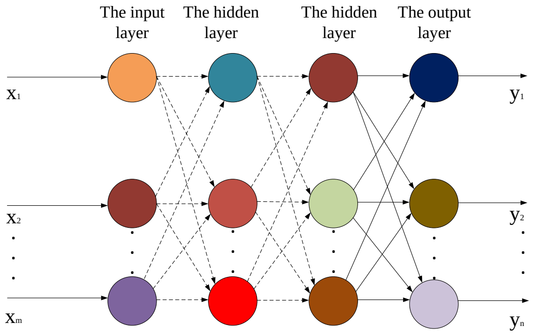

Figure 6. Multilayer feedforward neural network

5.2.2. Back propagation juris-rudence

The author considered a three-layer feedforward neural network with 'm' neurons in the input layer, 'l' neurons in the hidden layer and 'n' neurons in the output layer (Fig. 7). The weight symbol of the qth neuron of the hidden layer is 'v_q'. The weight of the ith neuron in the output layer is 'w_i' . The author has assigned the action function of the cells in the hidden layer. It is denoted by 'a_h(.)'. This function of the output layer and it is denoted by 'a_0(.)'. The relationship between the transmitted signals in the network as follows:

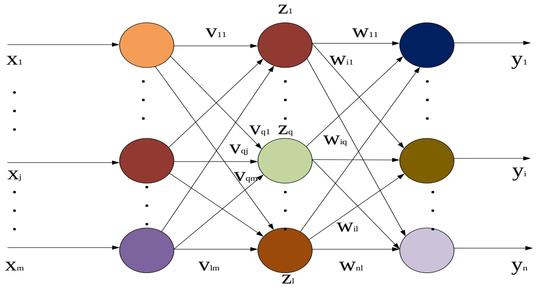

Figure 7. Three-layer feedforward neural network

The sum of the weights of the signals that enter the qth neuron in the hidden layer:

$$net_q=\sum_{j=1}^{m}v_{qj}x_j\tag{32}$$

Output signal of the qth neuron in the hidden layer

$$z_q=a_h(net_q)=a_h\left(\sum_{j=1}^{m}v_{qj}x_j\right)\tag{33}$$

The sum of the weights of the signals that enter the ith neuron in the output layer

$$\begin{gathered}net_q=\sum_{q=1}^{l}w_{iq}z_q=\sum_{q=1}^{l}w_{iq}a_h\left(net_q\right)\\ net_q=\sum_{q=1}^{l}w_{iq}a_h\left(\sum_{j=1}^{m}v_{qj}x_j\right)\end{gathered}\tag{34}$$

Output signal of the ith neuron in the output layer

$$\begin{gathered}y_i=a_0\left(net_i\right)=a_0\left(\sum_{q=1}^{l}w_{iq}z_q\right)\\ y_i=a_0\left(\sum_{q=1}^{l}w_{iq}a_h\left(net_q\right)\right)=a_0\left(\sum_{q=1}^{l}w_{iq}a_h\left(\sum_{j=1}^{m}v_{qj}x_j\right)\right)\end{gathered}\tag{35}$$

The author has a network training dataset including K samples x(k), d(k), k=1...K. The criterion for training the network is to minimize the error:

$$E(w,v)=\frac{1}{2}\sum_{i=1}^{n}\left(d_i-y_i\right)^2$$
$$E(w,v)=\frac{1}{2}\sum_{i=1}^{n}\left(d_i-a_0\left(net_i\right)\right)^2$$
$$E(w,v)=\frac{1}{2}\sum_{i=1}^{n}\left(d_i-a_0\left(\sum_{q=1}^{l}w_{iq}z_q\right)\right)^2$$
$$E(w,v)=\frac{1}{2}\sum_{i=1}^{n}\left(d_i-a_0\left(\sum_{q=1}^{l}w_{iq}a_h\left(net_q\right)\right)\right)^2 \tag{36}$$

Applying the gradient descent algorithm, the weights of the output layer are updated:

$$w_{iq}(k+1)=w_{iq}(k)-\eta\frac{\partial E(k)}{\partial w_{iq}} \tag{37}$$

$$\frac{\partial E(k)}{\partial w_{iq}}=\left[\frac{\partial E(k)}{\partial y_i}\right]\left[\frac{\partial y_i}{\partial net_i}\right]\left[\frac{\partial net_i}{\partial w_{iq}}\right]$$
$$\frac{\partial E(k)}{\partial w_{iq}}=\left[-\left(d_i(k)-y_i(k)\right)\right]\left[a_0\left(net_i(k)\right)\right]\left[z_q(k)\right] \tag{38}$$

The author has set

$$\delta_{oi}(k)=-\frac{\partial E(k)}{\partial net_i}=\left[\frac{\partial E(k)}{\partial y_i}\right]\left[\frac{\partial y_i}{\partial net_i}\right] \tag{39}$$
$$\delta_{oi}(k)=\left[d_i(k)-y_i(k)\right]\left[a_0\left(net_i(k)\right)\right]$$

The author has replaced (39) and (38) in (37)

$$w_{iq}(k+1)=w_{iq}^{*}(k)-\eta\delta_{oi}(k)z_q(k) \tag{40}$$

Similarly, the weight of the hidden layer is updated by the formula:

$$v_{qj}(k+1)=v_{qj}(k+1)-\eta\frac{\partial E(k)}{\partial v_{qj}} \tag{41}$$

$$\frac{\partial E(k)}{\partial v_{qj}}=\left[\frac{\partial E(k)}{\partial z_q}\right]\left[\frac{\partial z_q}{\partial net_q}\right]\left[\frac{\partial net_q}{\partial v_{qj}}\right]$$
$$\frac{\partial E(k)}{\partial v_{qj}}=\left[-\sum_{i=1}^{n}\left(d_i(k)-y_i(k)\right)a_0'\left(net_i(k)\right)w_{iq}(k)\right] \tag{42}$$
$$\times\left[a_h'\left(net_q(k)\right)\right]\times\left[x_j(k)\right]$$

The author has set

$$\delta_{hq}(k)=-\frac{\partial E(k)}{\partial net_q}=-\left[\frac{\partial E(k)}{\partial z_q}\right]\left[\frac{\partial z_q}{\partial net_q}\right]$$
$$\delta_{hq}(k)=\left[-\sum_{i=1}^{n}\left(d_i(k)-y_i(k)\right)a_0'\left(net_i(k)w_{iq}(k)\right)\right] \tag{43}$$
$$\times\left[a_h'\left(net_q(k)\right)\right]$$

The author has replaced (39) in (43)

$$\delta_{hq}(k)=\left[\sum_{i=1}^{n}\delta_{oi}(k)w_{iq}(k)\right]\left[a_h'\left(net_q(k)\right)\right] \tag{44}$$

The author has combined (41), (42) and (44)

$$v_{qj}(k+1)=v_{qj}(k)-\eta\delta_{hq}(k)x_j(k) \tag{45}$$

Since the weights of the network are updated based on the error signals $\left(\delta_{oi}(k),\delta_{hq}(k)\right)$ and they can be extended to networks with more layers of computational neurons, the back- propagation algorithm also known as the generalized Delta learning algorithm.

5.2.3. Multilayer feedforward neural network on Matlab

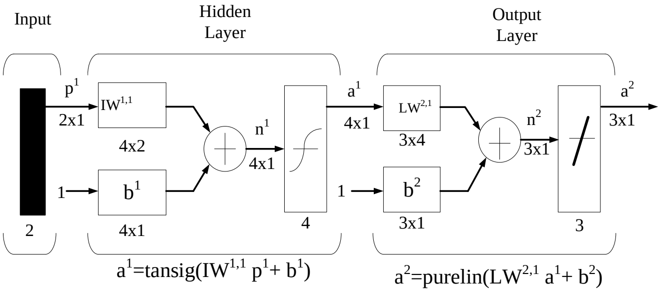

Figure 8. Model of Multilayer feedforward neural network on Simulink

To set up multilayer feedforward neural network below on Matlab, the author used the command 'newff', which takes four input arguments, the first is the value 'input' taken from the variable name 'in' of 'To workspace' in Simulink. This value indicates the range of the input variable, followed by arrays showing the number of neurons per layer: the first layer has fifty neurons, the output layer has one neuron, then the array showing the name of conversion functions used in each layer: the input layer conversion function is 'tan-sigmoid', the output layer is layer linearity, and finally the name of the function used to train the network: the training function is 'trainrp', parameters of the network are initialized according to preset algorithm. The command is described as follows: net= newff ([minmax (input)], [50 1], {'tansig' 'purelin'}, 'trainrp').

6. Simulation results and discussions

Simulation results are shown Figures 9, 10, 11, 12, 13, 14, 15, 16, 17, 18, 19, 20, 21.

Part 1: Model with using LQG regulator

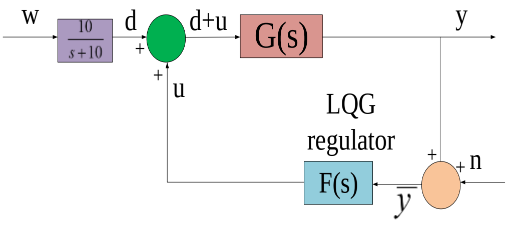

Figure 9. LQG regulator G(s)

Fig 9: the value of 'd' is a color noise signal with a spectral density of less than 10 rad/s, the value of 'n' is a white noise signal $E(n^2)=0.01$.The value of quality indicator 'J': $J(u)=\int_0^\infty (10y^2+u^2)dt.$

The model of the object:

$$\dot{x}=Ax+Bu+Bd, \quad \bar{y}=Cx+n$$

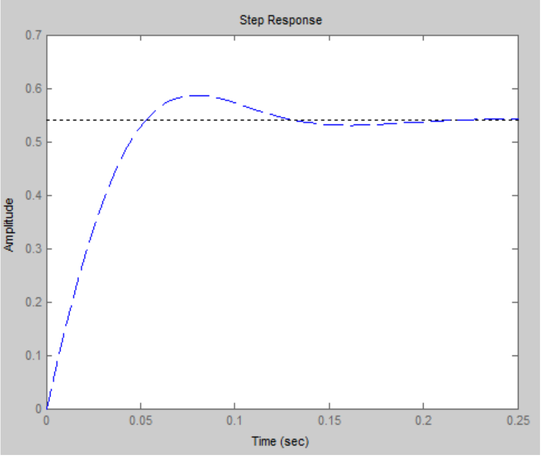

Figure 10. step response of the open loop 'G(s)

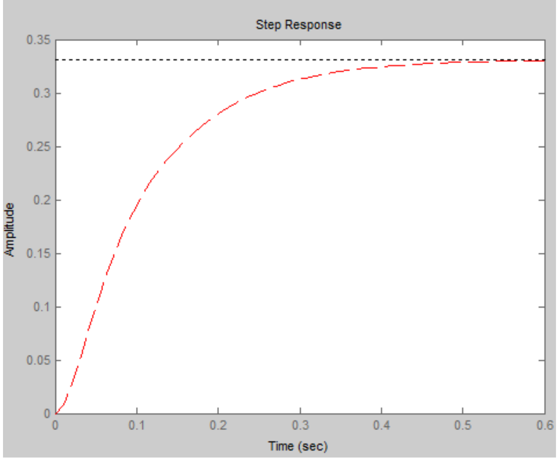

Figure 11. step response of the closed loop 'G(s)'

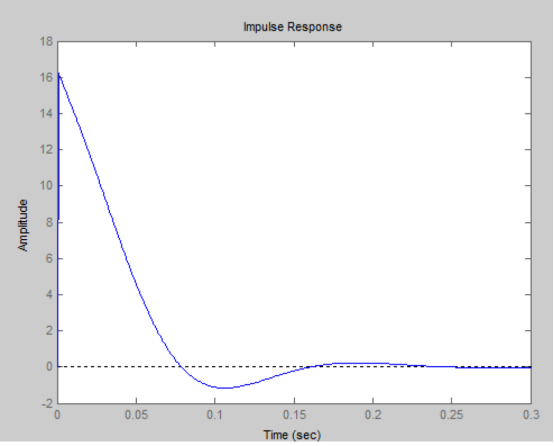

Figure 12. impulse response of the open loop 'G(s)'

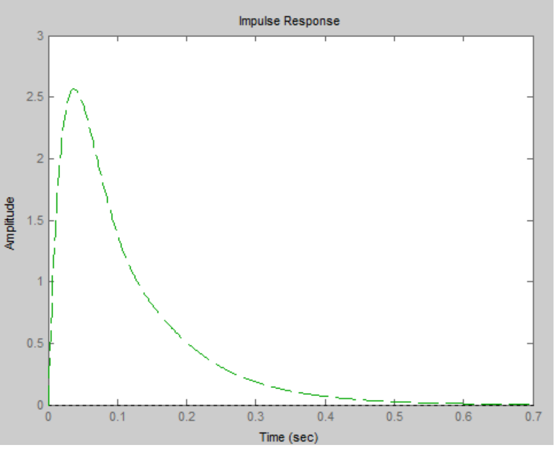

Figure 13. impulse response of the closed loop 'G(s)'

Figure 13: impulse response for the closed loop (the signal is highlighted in green) is worse than the open loop (the signal is highlighted in blue in Fig 12). The amplitude of the oscillation of the closed loop in this case is zero and the closed loop reaches a steady state. For LQG regulator, the closed loop responds well. The amplitude of the oscillation of the open loop in this case is large and the open system can reach a steady state. Figure 11: step response for the closed loop (the signal is highlighted in red) is better than the open loop (the signal is highlighted in green in Fig 10). The amplitude of the oscillation of the closed loop in this case is 0.35 and the closed loop reaches a steady state. For LQG regulator, the closed loop responds well. Meanwhile, the open loop can respond well.

Part 2: Model with using PID controller

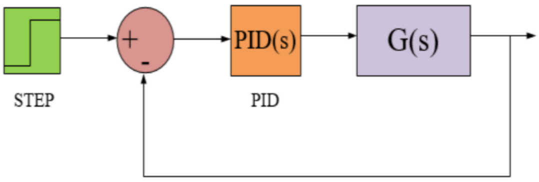

Figure 14. Simulink model of PID controller (K_p=56.71; K_i=46.1; K_d=562.44)

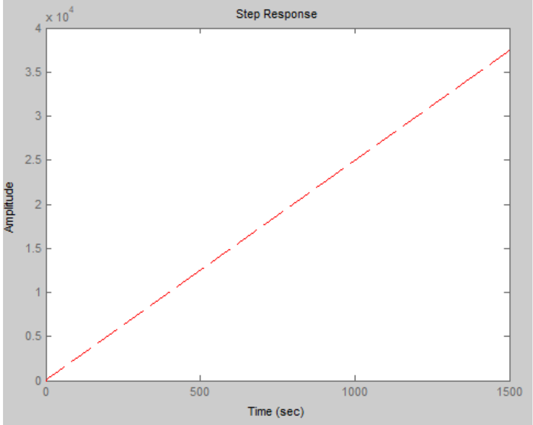

Figure 15. step response of the open loop ‘G(s)’

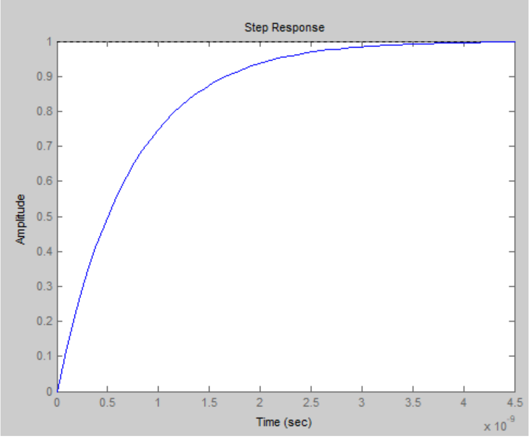

Figure 16. step response of the closed loop ‘G(s)’

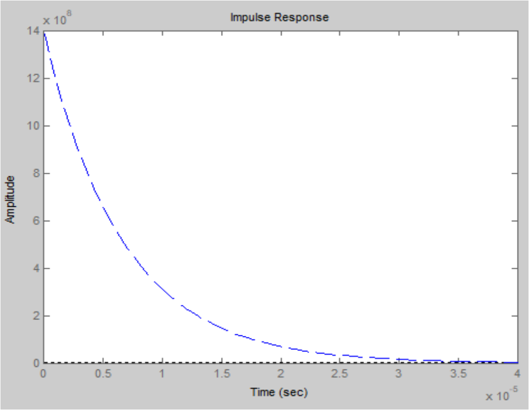

Figure 17. impulse response of the open loop ‘G(s)’

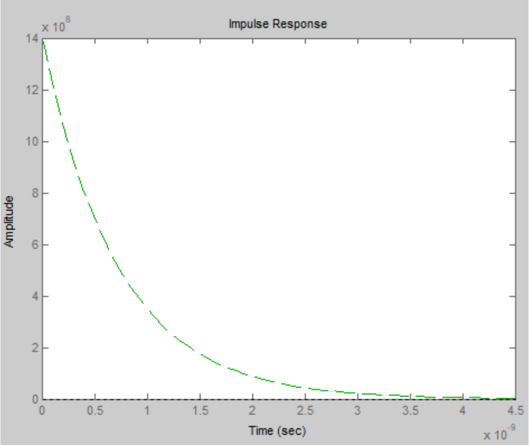

Figure 18. impulse response of the closed loop ‘G(s)’

Figure 18: impulse response for the closed loop (the signal is highlighted in green) is better than the open loop (the signal is highlighted in blue in Fig 17). The amplitude of the oscillation of the closed loop in this case is zero and the closed loop reaches a steady state. For PID controller, the closed loop responds well. The amplitude of the oscillation of the open loop in this case is large and the open loop can reach a steady state. Figure 16: step response for the closed loop (the signal is highlighted in blue) is better than the open loop (the signal is highlighted in red in Fig 15). The amplitude of the oscillation of the closed loop in this case is 1.0 and the closed loop reaches a steady state. For PID controller, the closed loop responds well. Meanwhile, the open loop can not respond well. The closed loop responds better than the open loop because the closed loop has been standardized by designed diagrams of PID controller.

Part 3: Model with using ANN

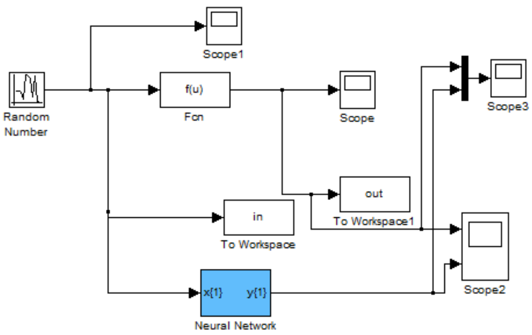

Figure 19. Simulink of model with using ANN

Step 1: The author has done a search for components on Simulink.

Step 2: The author has connected the components together as shown in the diagram.

Step 3: The author has programmed with the necessary commands to form the Neural Network (Blue box).

Step 4: The author has "played" the above diagram to get the results as shown in Figures 20, 21.

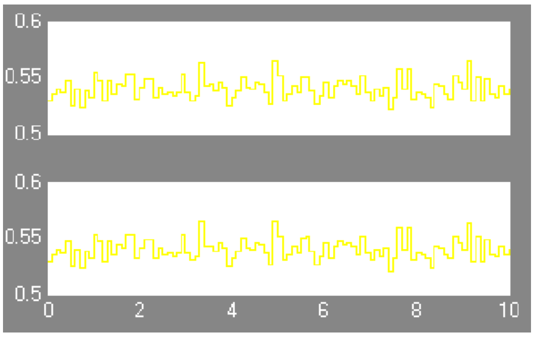

Figure 20. model with using ANN of Scope 2 ‘G(u)’

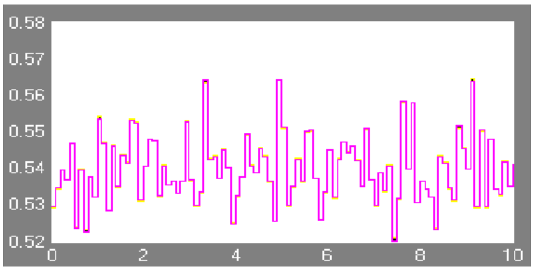

Figure 21. model with using ANN of Scope 3 ‘G(u)’

Figures 20, 21 are results of output values of the system. Figure 20 are the result of the value of the output without using ANN (above image) and Figure 20 also are the result of the output with using ANN (bottom image). Figure 21 are a composite image of the value of the output without using ANN and the value of the output with using ANN. This result has an almost absolute match between two values above. Therefore, this is considered a successful survey in training the network to achieve desired results. Efficiency levels are listed in descending order below with using above control methods. This is based on states that are determined to be stable through simulation results. The number of simulation results reaching steady state is the criterion to evaluate the effectiveness of PID controller, LQG regulator, ANN applied to the above model:

A. ANN (Figures 20, 21)
B. LQG regulator (Figures 10, 11, 12, 13)
C. PID controller (Figures 16, 17, 18)

Limitations of the proposed method: this proposal has not been widely recognized because topics of this type have never been published to readers. The attractiveness of the article is limited because the author is not fully equipped with comprehensive knowledge. In the future, themes of this genre need to be taken for other models with more and more sophisticated precision.

7. Conclusions

LQG regulator in case of noise signals affecting this system has been proposed by the author. Simulation results have been accepted for positive results. This allows the closed system to reach steady state in a long time. In fact, there are many noise signals affecting the system due to the working environment of the system. This can affect the output quality of a plan. PID controller in this case is considered to be more efficient than LQG regulator because the time to stabilize the system has been shortened. However, these two methods can not completely solve the instability of the open system. ANN in the case has achieved the expected positive result: the security of the system has been installed. Only users can perform operations on the system through applications of artificial intelligence. In the future, LQG regulator can be implemented on systems to address disadvantages and advantages as the author described above. Other interesting results can be noted by the author in other models that the author can investigate them.

References

[1] Abdo, M., Vali, A.R., Toloei, A.R., and Arvan, M.R. (2014). Modeling control and simulation of two axes gimbal seeker using fuzzy PID controller. In 2014 22nd Iranian Conference on Electrical engineering (ICEE), 1342–1347. doi: 10. 1109/ Iranian CEE. 2014. 6999742.

[2] Abdo, M.M., Vali, A.R., Toloei, A.R., and Arvan, M.R. (2014). Stabilization loop of a two axes gimbal system using self-tuning PID type fuzzy controller. ISA Transactions, 53(2), 591 602. doi: https:// doi.org/10.1016/j.isatra.2013.12.008.

[3] Abdo, M.M., Vali, A.R., Toloei, A.R., and Arvan, M.R. (2015). Improving two axes gimbal seeker performance using cascade control approach. Proceedings of the Institution of Mechanical Engineers, Part G: Journal of Aerospace Engineering, 229 (1), 38–55. doi: 10. 1177/ 0954410014525130

[4] Ahi, B. and Nobakhti, A. (2018). Hardware implementation of an ADRC controller on a gimbal mechanism. IEEE Transactions on Control Systems Technology, 26(6), 2268–2275. doi:10.1109 /TCST. 2017. 2746059.

[5] Caponetto, R. and Xibilia, M.G. (2017). Fractional order PI control of a gimbal platform. In 2017 European Conference on Circuit Theory and Design (ECCTD), 1–4. doi:10.1109/ECCTD. 2017. 8093271. 32 Jitendra Sharma et al. / IFAC PapersOnLine 53-1 (2020) 27–32.

[6] Chen, X., Cai, Y., Ren, Y., Yang, X., and Peng, C. (2019). Spacecraft angular rates and angular acceleration estimation using single-gimbal magnetically suspended control moment gyros. IEEE Transactions on Industrial Electronics, 66(1), 440–450. doi:10.1109/TIE.2018.2826468.

[7] Cui, P., Zhang, D., Yang, S., and Li, H. (2017). Friction compensation based on time-delay control and internal model control for a gimbal system in magnetically suspended CMG. IEEE Transactions on Industrial Electronics, 64(5), 3798–3807. doi: 10.1109/TIE.2016.2644620.

[8] Ding, Z., Zhao, F., Lang, Y., Jiang, Z., and Zhu, J. (2019). Anti-disturbance neural-sliding mode control for inertially stabilized platform with actuator saturation. IEEE Access, 7, 92220–92231. doi: 10. 1109/ACCESS. 2019. 2927427.

[9] Fang, J. and Ren, Y. (2011). High-precision control for a single-gimbal magnetically suspended control moment gyro based on inverse system method. IEEE Transactions on Industrial Electronics, 58 (9), 4331–4342. doi: 10. 1109/TIE. 2010. 2095394.

[10] Guo, Q., Liu, G., Xiang, B., Wen, T., and Liu, H. (2016). Robust control of magnetically suspended gimbals in inertial stabilized platform with wide load range. Mechatronics, 39, 127– 135. doi: https:// doi.org/10.1016/j.mechatronics.2016.08.003.

[11] Huang, L., Wu, Z., and Wang, K. (2018). High-precision anti-disturbance gimbal servo control for control moment gyroscopes via an extended harmonic disturbance observer. IEEE Access, 6, 66336–66349. doi: 10. 1109/ ACCESS. 2018. 2878623.

[12] Jia, R., Nandikolla, V.K., Haggart, G., Volk, C., and Tazartes, D. (2017). System performance of an inertially stabilized gimbal platform with friction, resonance, and vibration effects. Journal of Nonlinear Dynamics, 2017.

[13] Kim, S.B., Kim, S.H., and Kwak, Y.K. (2010). Robust control for a two-axis gimbaled sensor system with multivariable feedback systems. IET Control Theory Applications, 4(4),539–551. doi:10.1049/iet-cta.2008.0195.

[14] Lee, H.P. (2019). Robust control of a two-axis gimbaled seeker using loop shaping design procedure. In 2019 20th International Carpathian Control Conference (ICCC), 1–6. doi: 10. 1109/ Carpathian CC. 2019. 8766056.

[15] Li, H., Ning, X., and Han, B. (2017a). Composite decoupling control of gimbal servo system in doublegimbaled variable speed CMG via disturbance observer. IEEE/ASME Transactions on Mechatronics, 22(1), 312–320. doi: 10. 1109/ TMECH. 2016.2601340.

[16] Li, H., Zheng, S., and Ning, X. (2017b). Precise control for gimbal system of double gimbal control moment gyro based on cascade extended state observer. IEEE Transactions on Industrial Electronics, 64(6), 4653–4661. doi: 10. 1109/ TIE. 2017. 2674585.

[17] Li, H., Ning, X., and Han, B. (2017). Speed tracking control for the gimbal system with harmonic drive. Control Engineering Practice, 58, 204 – 213. doi: https:// doi.org /10.1016 /j. conengprac. 2016. 11. 001.

[18] Li, H., Yang, S., and Ren, H. (2016). Dynamic decoupling control of DGCMG gimbal system via state feedback linearization. Mechatronics, 36, 127 – 135. doi: https:// doi.org /10. 1016/ j. mechatronics. 2016. 04. 004.

[19] Majumder, C.G., Kumar, K.A., Siva, M.S., and Philip, N. (2018). Integrated gimbal dynamics model for precise gimbal rate control in single gimbal-CMG to achieve high accuracy pointing. IFAC-Papers On Line, 51(1), 713 – 718. doi: https: //doi. org/10.1016/j. ifacol. 2018. 05. 120. 5th IFAC Conference on Advances in Control and Optimization of Dynamical Systems ACODS 2018.

[20] Obiora, V. and Achumba, I.E. (2017). Adaptive control of aerial vehicle gimbal using fuzzy- PID compensator. In 2017 IEEE 3rd International Conference on ElectroTechnology for National Development (NIGERCON), 451–456. doi: 10. 1109 /NIGERCON. 2017. 8281914.

[21] Rajesh, R.J. and Ananda, C.M. (2015). PSO tuned PID controller for controlling camera position in UAV using 2-axis gimbal. In 2015 International Conference on Power and Advanced Control Engineering (ICPACE), 128–133. doi: 10.1109/ ICPACE. 2015. 7274930.

[22] An Enhanced GRU Model With Application to Manipulator Trajectory Tracking, EAI Endorsed Trans AI Robotics, vol. 1, no. 1, p. e1, 2022.

[23] Briefly Revisit Kinematic Control of Redundant Manipulators via Constrained Optimization, EAI Endorsed Trans AI Robotics, vol. 1, no. 1, p. e4, 2022.

[24] Incorporation of efficient second-order solvers into latent factor models for accurate prediction of missing Q$_o$S data, IEEE Trans. on Cybernetics, vol. 48, no. 4, pp. 1216-1228, 2018.

[25] An Overview of Calibration Technology of Industrial Robots, IEEE/ CAA J. Autom. Sinica, vol. 8, no. 1, pp. 23-36, Jan. 2021.

[26] Diversified Regularization Enhanced Training for Effective Manipulator Calibration, IEEE Transactions on Neural Networks and Learning Systems, doi: 10.1109/TNNLS.2022.3153039.